Anodic Growth of Large-Diameter Multipodal TiO_2 Nanotubes

Arash Mohammadpour,[†] Prashant R. Waghmare,[‡] Sushanta K. Mitra,[‡] and Karthik Shankar[†,*]

[†]Department of Electrical & Computer Engineering, University of Alberta, Edmonton, AB T6G 2 V4 Canada, and [‡]Micro and Nano-Scale Transport Laboratory, Department of Mechanical Engineering, University of Alberta, Edmonton, Canada T6 G 2G8

ABSTRACT We report on the formation of a new class of nanostructures, namely, multipodal hollow titania nanotubes possessing two or more legs, achieved during the electrochemical anodization of titanium in diethylene glycol (DEG)-based electrolytes. The unique multipodal porous structure is expected to extend and enhance the applications of TiO_2 nanotube arrays. Multipodal nanotubes form by a process we term "nanotube combination", which only occurs in viscous electrolytes at high anodization potentials in the presence of a low concentration of fluoride-bearing species. The mechanism of formation of multipodal nanotubes is considered, and the tube length at which nanotube combination occurs is predicted theoretically using a simplified analytical model. The results suggest that capillary forces strong enough to bend the TiO_2 nanotubes by tens of degrees are generated during the imbibition of electrolyte into and out of the intertubular spaces between adjacent tapered nanotubes.

KEYWORDS: self-organization · tapered nanotubes · nanopores · nanofluidics · tetrapods · capillary forces · surface tension · dynamic contact angle

The n-type semiconducting, vertically oriented, self-organized TiO_2 nanotube arrays formed by electrochemical anodization constitute a mechanically robust, high surface area, easily functionalized architecture with vectorial electron percolation pathways.[1,2] Consequently, they have demonstrated superior performance as gas sensors,[3,4] photocatalysts,[5,6] and also scaffolds for excitonic solar cells.[7−9] Other promising applications, where the tubular structure and tunable pore size of TiO_2 NT arrays are the properties of interest, include drug eluting coatings for medical implants,[10] solid-phase microextraction (SPME) fibers,[11] and stem cell differentiation.[12,13] Despite the impressive progress in tuning the length, wall thickness, diameter, and pattern order of anodically formed TiO_2 NT arrays, there is still an unmet need for more complex hierarchical nanostructures which not only improve their functionality in present applications but also make novel applications possible.[14] Applications and techniques which rely on volumetric filling or surface functionalization of nanotubes[15−19] will particularly benefit from the production of multipodal nanotubes with a more complex topology. The differential chemical functionalization of the individual legs allows for multiplexed sensing and the loading of multiple drugs. Moreover, since the multipodal structure provides more than one leg for each of the nanotubes, a more robust attachment of nanotubes onto desired substrates is possible, which also renders them good load-bearing elements for mounting heavier structures. The branched topology of multipodal titania nanotubes consisting of a large diameter nanotube dividing at the end into several smaller size nanotubes could be applied for molecular separation in a multiphase multicomponent fluid and for microfluidic and optofluidic applications. The multipodal topology also lends itself to use in three-terminal devices, electrical interconnect networks, and nanoelectromechanical systems.[20] The syntheses and applications of multipodal quantum dots—mainly tetrapodal nanocrystals of II−VI semiconductors such as ZnO, CdS, and CdTe[21]—are a focus of intense research activity. The multipodal structure is highly advantageous in applications such as photocatalysis[22] and photovoltaics[23] due to the larger surface-to-volume ratio and more facile charge separation at the core−leg interfaces.

RESULTS AND DISCUSSION

To the best of our knowledge, multipodal titania nanotubes have not been reported so far. Herein we report on the production of multipodal titania nanotubes (see Figure 1) which result from a newly introduced process that we call *nanotube combination*. Almost every nanotube in the images of Figure 1a and Figure 1b is at least

*Address correspondence to kshankar@ualberta.ca.

Received for review October 3, 2010 and accepted November 05, 2010.

Published online December 3, 2010. 10.1021/nn1026214

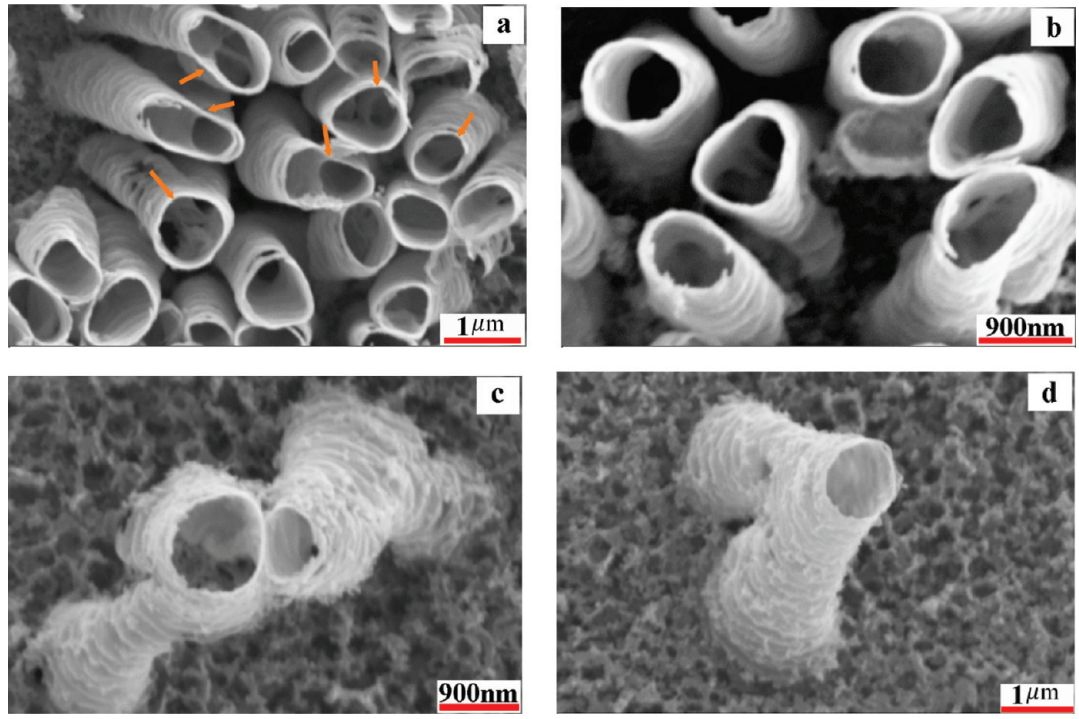

Figure 1. SEM images of multipodal titania nanotubes anodized in a DEG electrolyte with 0.25% HF and 2% water (a) at 120 V for 44 h, (b) at 120 V for 47 h, and (c,d) at 150 V after 47 h. Arrows in panel a point to easily identifiable multipodal nanotubes not obscured by the topology or tilt angle.

bipodal. Figure 1c shows two bipodal nanotubes in the process of forming a tetrapodal nanotube, while Figure 1d is a tetrapodal nanotube, which appears bipodal at first glance because the process of nanotube combination for the constituent bipodal nanotubes is complete. We propose a mechanism that explains the formation of multipodal nanotubes and also explains some of the unique features associated with the growth of TiO_2 nanotube arrays in diethylene glycol (DEG)-based electrolytes. Anodization in DEG-based electrolytes exhibits some unusual features such as the formation of nanotubes with very large pore sizes (up to 900 nm)[24] and discretization of nanotubes by large intertubular spacings,[24−26] a deviation from the close-packed architecture found in other electrolytes. Our studies indicate that the process of nanotube combination has a decisive role in the simultaneous increment of the both pore size and intertubular spacing of nanotube arrays anodically formed in a HF containing DEG electrolyte.

Field-assisted oxide dissolution and cation migration, field-assisted oxidation of Ti, and chemical etching are the competing reactions responsible for the growth of TiO_2 nanotube arrays (a key difference from the formation of nanoporous alumina, in which only the field-assisted processes are important). The field-assisted reactions occur on either side of the barrier layer at the bottom of the nanotubes and are responsible for driving the Ti/TiO_2 interface deeper into the Ti foil, a process that increases the length of the nanotubes. Chemical etching shortens the length of the nanotubes.[27,28]

$$\text{field-assisted oxidation: } Ti + 2H_2O \rightarrow TiO_2 + 4H^+ + 4e^- \quad (1)$$

$$\text{field-assisted migration: } Ti^{4+} + 6F^- \rightarrow [TiF_6]^{2-} \quad (2)$$

$$\text{field-assisted dissolution: } TiO_2 + 6F^- + 4H^+ \rightarrow [TiF_6]^{2-} + 2H_2O \quad (3)$$

$$\text{chemical dissolution: } TiO_2 + 6HF \rightarrow [TiF_6]^{2-} + 2H_2O + 2H^+ \quad (4)$$

Nanotubes formed in HF-bearing DEG-based electrolytes at large anodization potentials exhibit a definite taper with a wider base and a narrower mouth, as shown in Figure 2a. The taper occurs as a consequence of the significant variation in the conductivity of the electrolyte, which occurs over the course of the anodization process. The low conductivity of the DEG-based electrolyte has been remarked upon by others[25] and occurs due to a combination of three factors: (a) the high viscosity of DEG and the concominant low ionic mobilities;[29] (b) low concentration of ionic charge carriers due to low dissociation of the weak acid (HF); and (c) large hydrodynamic radius of dissociated ions due to solvation[30] by water and DEG molecules. As the anodization of Ti proceeds, the concentration of $(TiF_6)^{2-}$ ions increases with time due to the chemical reactions represented by eqs 2, 3, and 4. Due to a more delocalized distribution of charge in the complex,[31] $(TiF_6)^{2-}$ ions are

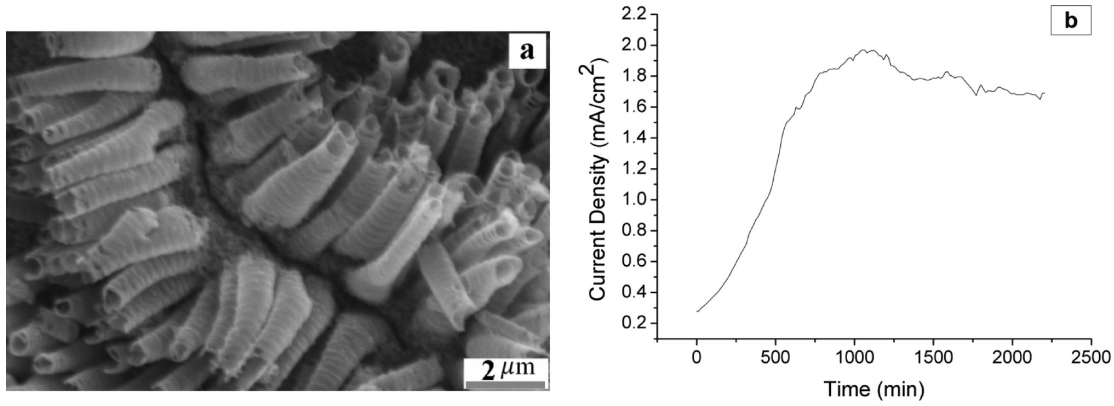

Figure 2. (a) SEM image of the cross section of titania nanotubes formed by anodization at 120 V in a DEG electrolyte with 0.25% HF and 1% water, showing a clear taper from mouth to base. (b) Anodic current density as a function of anodization time for 120 V anodization identical DEG electrolyte (0.25% HF and 1% water).

also less solvated and therefore more mobile. Consequently, the conductivity of the electrolyte increases with anodization duration, which manifests itself in a higher anodization current density at the same potential, an effect clearly seen in the anodization current transient plot of Figure 2b, during the first 20 h of anodization. The increase in the conductivity of the electrolyte makes a large proportion of the applied anodization potential available for the anodization process since the potential drop across the electrolyte (anodization current $i \times$ electrolyte resistance R) reduces with time. Therefore, the base of the nanotubes which form later in the process experiences higher effective anodization voltages than the top (mouth) of the nanotubes, which are formed relatively early in the process. Due to the well-known dependence of the diameter of the nanotubes on the anodization voltage, a tapered nanotube morphology wider at the base than at the top is produced.

The field-assisted oxidation process generates H^+ ions according to eq 1 and results in local acidification at the pore bottom.[32] On the other hand, F^- ions are consumed by dissolution reactions. Therefore, while F^- concentration is maximum at the mouth of the tubes (nearly equal to concentration in the bulk electrolyte) and drops to a minimum at the pore bottom, H^+ ion concentration is maximum at the pore bottom and decreases toward the mouth of the tubes. Such a fluoride ion concentration gradient along the length of the nanotubes has been confirmed by compositional analysis using X-ray photoelectron spectroscopy (XPS).[33] It is also fairly well-known that less fluoride results in a thick oxide layer which suppresses the transport of titanium, oxygen, and fluorine ions, and excess fluoride results in a thin oxide layer that enhances the transport of titanium, oxygen, and fluorine ions, thus inducing inward growth faster.[34] Nanotube length increases so long as the rate of movement of the Ti/TiO_2 interface is faster than the rate of loss of TiO_2 NTs by chemical etching. The anodization current is roughly proportional to the strength of the field-assisted reactions and is thus indicative of the rate at which the Ti/TiO_2 interface is moving into the Ti foil.[35] As shown in Figure 2b, the anodization current increases for the first ~20 h of anodization and then decreases nearly monotonically. As discussed previously, the increase in anodization current occurs due to an increase in electrolyte conductivity. Thus the rate of movement of the interface peaks ~20 h into the anodization process and declines thereafter due to a paucity of fluoride ions at the pore bottom. At this point in the anodization process, field-assisted dissolution weakens relative to field-assisted oxidation, resulting in an increase in the thickness of the barrier layer. The thicker barrier layer retards the solid state ionic transport of reactants through the barrier layer and causes a decrease in the anodization current density. If purely high-field ionic conduction was involved, then the current would be expected to continuously decrease with time. If this was purely a mass transfer limited process, the anodization current would be expected to level off instead of decreasing. In our scheme, the anodization reaction is under mixed control of the high-field solid state ionic transport and mass transport. Chemical etching, in contrast, is relatively constant and becomes more dominant as the anodization current decreases.

We propose a mechanism that explains our observations and accounts for the unique formation of multipodal TiO_2 nanotubes in HF/DEG/water electrolytes. As mentioned previously, a gradient in fluoride-bearing species exists along the length of the growing nanotube, with the highest concentration corresponding to that of the bulk existing at the mouth of the tube and decreasing toward the barrier layer. Consequently, in the first 20 h of the anodization process, when nanotubes are increasing in length, chemical etching, even though isotropic, only shortens the height of the nanotubes by etching from the top. The solid state transport of reactant ions through the barrier layer occurs through a high-field process exponentially dependent on the electric field across the barrier layer and therefore sensitive to barrier layer thickness. When the anodization current begins to decrease after 20 h, there is in-

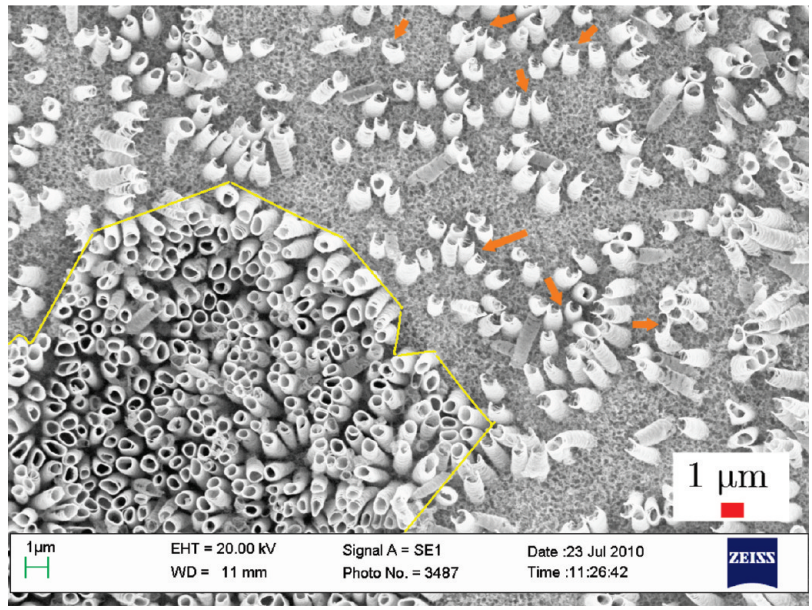

Figure 3. SEM images of the surface of a Ti foil anodized in a DEG-based electrolyte containing 0.25% HF and 1% H_2O for 43 h at 120 V. Two distinct regions consisting of close-packed and widely separated nanotubes are demarcated by the yellow border.

creased competition for the lower current from all of the nanotubes and minor variations in barrier layer thickness play a significant role in allocating current among nanotubes. As chemical etching becomes more dominant, nanotubes in regions where the barrier layer is slightly thicker grow into the Ti foil more slowly but experience the same rate of chemical etching, thus gradually becoming shorter than nanotubes in regions where the barrier layer is slightly thinner. Due to the tapered structure of the nanotubes, a decrease in the height of such nanotubes also increases intertubular spaces where the viscous bulk electrolyte (richer in fluoride) can now penetrate—thus the same nanotubes experience more accelerated rates of dissolution due to chemical attack from the sides in addition to etching from the top. Soon, these nanotubes are completely consumed. Also, since the Ti/TiO_2 interface in the regions of thicker barrier layer moves into the metal more slowly, these regions are gradually more elevated with respect to adjacent regions with a thinner barrier layer. This effect is clearly seen in Figure 3, which shows two such regions adjacent to each other. The region enclosed by the yellow border in Figure 3 has relatively close-packed nanotubes as well as dark regions indicative of depth and greater topographic contrast. The barrier layer is visible in the region outside the yellow border, which is lighter on account of being at a higher elevation. In this elevated region, several nanotubes have been consumed by chemical etching, resulting in a wider separation. Several of the still-remaining nanotubes in this region have experienced severe side wall etching (some of these are pointed out by the orange arrows in Figure 3).

Figure 4 shows SEM images of the obtained titania nanotube arrays at different anodization times. After 40 h of anodization (Figure 4a), the nanotubes are still fairly close-packed, but from this point onward, chemical etching becomes dominant. From Figure 4b−d, it can be clearly seen that the nanotube structures become successively less close-packed in the course of the next few hours, resulting in a dramatic decrease in the areal density of nanotubes on the substrate. The absence of side wall chemical etching in the regions of closely packed nanotubes preserves those nanotubes.

Nanotubes of very large diameter (extending to optical and near-infrared wavelengths) may be obtained in DEG electrolytes,[24] as seen in Figure 5a,b. Two concurrent processes are responsible. Although closely packed nanotubes do not undergo significant chemical etching of their side walls, they do experience etching from the top, which shortens them because of the presence of the electrolyte at their mouth. In process I, nanotubes of large pore size are formed by the top-etching process, which increases their diameter due to their tapered conical shape. In process II, nanotubes of large pore size form by the combination of small pore size ones. As shown in the diagram of Figure 5c, the pore size of both process I (individual nanotubes) and process II (multipodal nanotubes) was increased for longer anodization times subsequent to the formation of the self-organized nanotubular structures on the surface, growing from just more than 300 nm after 40 h of anodization to about 900 nm after 47 h for combined nanotubes. The reason for the pore size increment of the process I nanotubes is shown schematically in Figure 5d. The nanotube combination process is schematically shown in Figure 5e, in which Figure 5e (step I) rep-

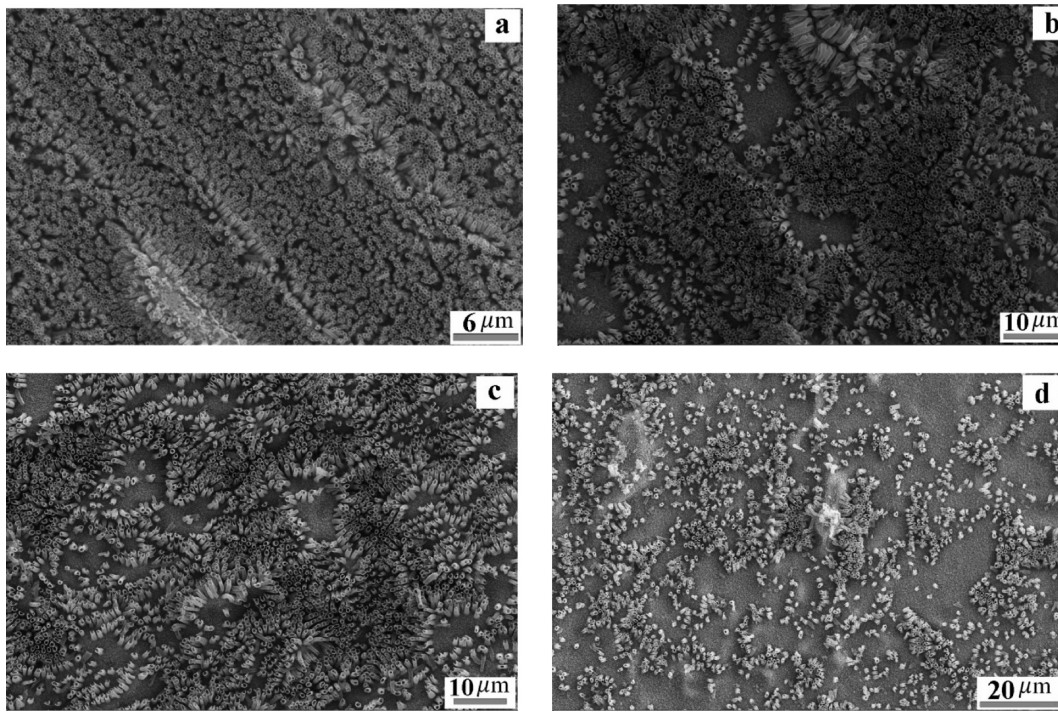

Figure 4. SEM images of titania nanotubes anodized at 120 V in a DEG electrolyte with 0.25% HF and 1% water after (a) 40 h, (b) 43 h, (c) 45 h, and (d) 47 h.

resents the common surface area of the two leaning nanotubes. Like ethylene glycol (EG) and water, DEG is a highly structured solvent with a three-dimensional spatial network of hydrogen bonds. It is known that H^+ ions, OH^- ions, and glycoxide ions have anomalously high conductance and mobility in these electrolytes due to the proton jump mechanism. Halide ions, on the other hand, have much lower conductance and mobility in EG and DEG.[36,37] A consequence of this asymmetry is that hydroxyl ions and glycoxide ions consumed at the Ti/TiO_2 interface during oxidation are replenished from the bulk electrolyte more quickly than fluoride ions consumed in the electrochemical dissolution of the barrier layer, and this asymmetry becomes more pronounced as nanotube length increases. Also, the bulkier $[TiF_6]^{2-}$ ions produced at the pore bottom do not disperse quickly into the bulk electrolyte due to their low mobility in the viscous electrolyte and their Coulombic attraction to the anode. It should be mentioned that the chemical etching at the nanotube mouth occurs continuously and the high viscosity of the electrolyte limits the long distance movement of the dissolved material, which increases its concentration in the electrolyte/nanotube interface region. As depicted in Figure 5e (step II), this highly saturated electrolyte etches both the side wall and interface between the leaning nanotubes, the small amount of saturated electrolyte at the mouth becomes supersaturated, and additional dissolved nanotube material becomes deposited onto the inner surface of the nanotube (the electrolyte/nanotube interface). Hence, the side wall becomes thicker, which results in the reduction of in chemical etching rate *relative* to that of the nanotube interwall. The SEM images in Figure 5a,b clearly show this stage after 45 h anodization with the same electrolyte mentioned before. According to Figure 5e (step III), the difference in the chemical etch rate dissolves the interwall deeper into the nanotube, which results in the combination of nanotubes leaning toward each other, as seen in the SEM image in Figure 1d for 47 h of anodization.

As can be seen in Figure 5a,b, if the leaning nanotubes possess a larger interface from top to bottom, the resulting combined nanotube looks like a single large pore size nanotube; otherwise, it would be a multipodal large diameter nanotube having several legs depending on the number of combined nanotubes. Less than 40 h of anodization resulted in a closely packed compact nanotube architecture. To investigate the effect of the presence of electric field in preserving the nanotubes against the chemical etching, the electric field was removed after 40 h of anodization, and the results for different etching times are provided in Supporting Information. It can be clearly seen from Figure 5a that, during the first hour after voltage removal, the combination process was at its initial stage and the interwall between the nanotubes is still visible and has not etched very deeply into the nanotubes. Nevertheless, at longer times, the nanotubes are completely etched and an irregular film is redeposited from the supersaturated electrolyte (Figures S1−S3).

It is clear from SEM images, such as those in Figure 1c,d and Figure 4a,b, that the nanotubes bend before combining. Bending and bunching of high aspect ratio

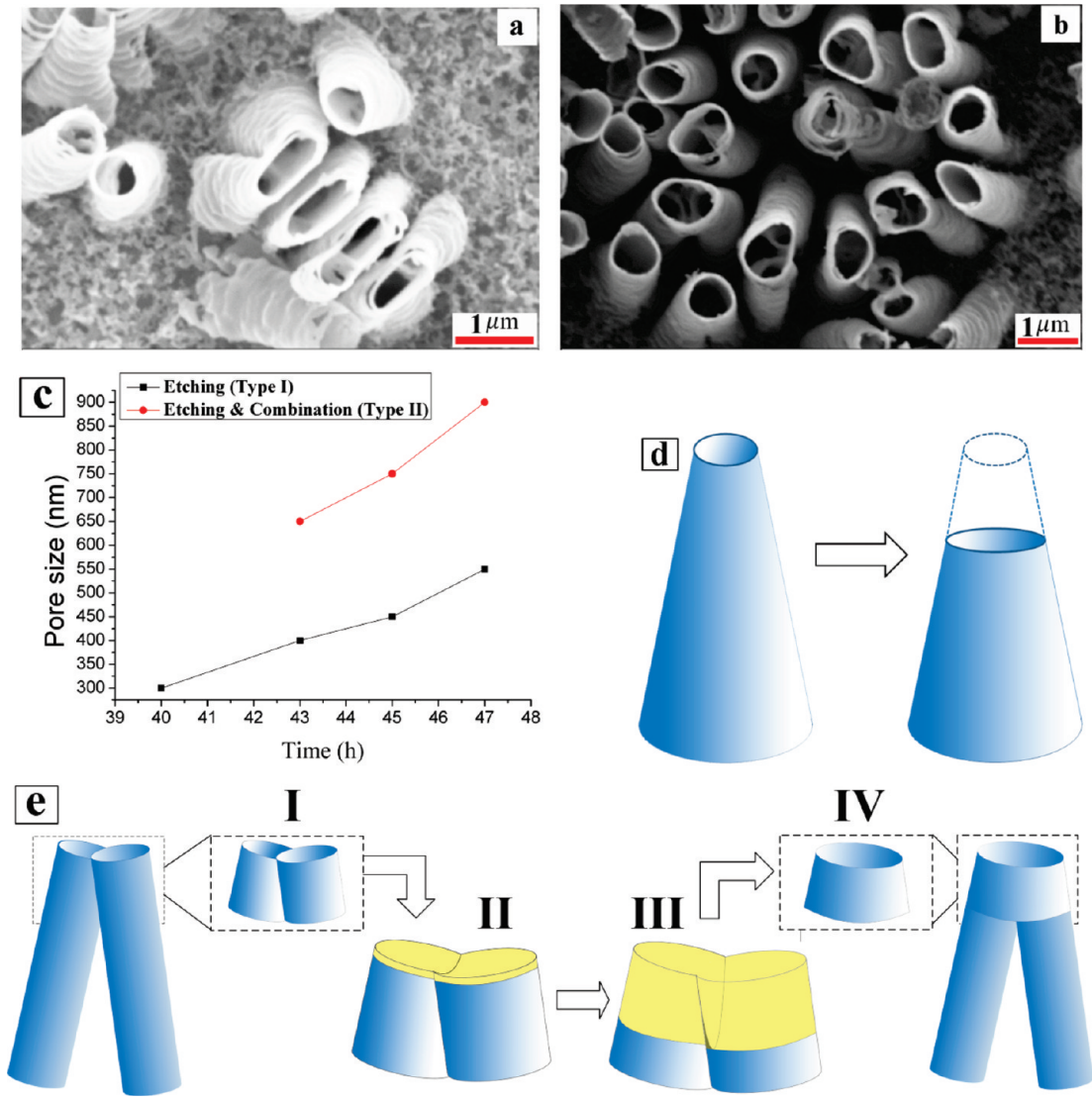

Figure 5. SEM images of titania nanotubes anodized at 120 V in a DEG electrolyte with 0.25% HF and 1% water (a) after 45 h of anodization and 1 h in the same bath without electric field. Four consecutive bipodal nanotubes can be seen and (b) top view after 45 h of anodization. (c) Pore size increment diagram of the individual and combined nanotubes *vs* anodization time and schematic image of the pore size increment in (d) individual and (e) combined nanotubes.

(AR > 150) TiO_2 nanotubes grown in fluoride-ion-bearing glycerol−water electrolytes has been previously observed due to surface tension effects during the drying process. By supercritical drying in CO_2, such bending has been minimized or even eliminated.[38] The nanotubes formed in the present study have much lower aspect ratios of ~5−25, therefore implying that the force causing the bending is much larger. We present a theoretical analysis to support the bending of nanotubes to form bipodal nanotubes based on the calculation of deflection of the nanotube due to the capillary force on its surface. The capillary force is exerted on the nanotubes by the wetting of the electrolyte during the growth of the nanotubes. With high-viscosity ionic liquids, Roy *et al.*[39] found that preferential wetting occurred in the intertubular spaces of TiO_2 nanotube arrays. Furthermore, hardly any penetration of the ionic liquid into the nanotubes occurred even after 5 h, whereas the intertubular spaces were wetted. The wetting in such a scenario takes place preferentially between the nanotubes only, and the electrolyte penetration into the nanotubes is minimal.[39] In the present study using highly viscous DEG electrolytes, it is assumed that such wetting takes place along the circumference of the tubes only, which creates a circumferential interface formed between the nanotubes. The separation distance between the nanotubes is termed as the base separation distance (BSD). On the basis of the wetting properties of the electrolyte and the surface of the nanotubes, such as the surface tension of the electrolytes and contact angle of the same electrolyte with the nanotube surface, one can determine the capillary force as

$$F_c = \pi \gamma_{LV} \sin\theta \sin\phi D_o^t$$

where, γ_{LV} is the surface tension of electrolyte, θ is the

static equilibrium contact angle of the electrolyte with the nanotube surface, ϕ is the taper angle of the nanotube at the base, and D_o^t is the outer diameter of the nanotube at distance L from base, that is, at the tip of the nanotube. It is assumed that this is the only force responsible for the deflection of the nanotube at the tip. One can determine the deflection of the nanotube of Young's modulus E with capillary force as the prescribed load at the tip as follows

$$\delta_t = \frac{F_c L^3}{3EI}$$

where the moment of inertia I can be determined with the geometrical dimensions of the nanotubes. As-anodized TiO_2 nanotubes are amorphous. The density of amorphous TiO_2 is known to vary from 3.0 to 4.0 depending on the conditions of growth.[40] We calculated the deflection of titania nanotubes in DEG due to capillary forces for limiting cases of the density of amorphous TiO_2, 3.88 g cm^{-3} representative highly dense TiO_2 tube walls and 3.0 g cm^{-3} for the condition of amorphous TiO_2 of much lower density.

Figure 6 shows the variation in the deflection of the nanotube with different contact angles of the electrolytes. The point of attachment is the length at which the deflection of the nanotube crosses half the distance between the nanotubes (*i.e.*, 0.5 times the tip separation distance (TSD)). The tapered configuration of the nanotubes has a direct bearing on the calculation of I and the capillary force. It is observed that for lower contact angle, that is, 20° with surface tension of 0.06 N/m, the magnitude of the deflection is too small to achieve the point of attachment. Further increment in the contact angle increases the deflection for the same length of the nanotube. Under the assumption that the amorphous TiO_2 constituting the nanotube walls is highly dense (ρ = 3.88 g cm^{-3}), the point of attachment is obtained for a contact angle of 70° and a tube length of 1.17 μm. When the amorphous TiO_2 is assumed to be less densified (ρ = 3.0 g cm^{-3}), the nanotubes are easier to deflect. Therefore, for this case, the point of attachment occurs at a much lower contact angle of 50° but the tube length remains very similar at 1.09 μm. The exact nanotube length at which combination occurs is not known; however, the point of attachment is inferred from SEM images to be in the range of ~1−2 μm, which supports the present analysis. It is to be noted that the measured value of the surface tension of electrolyte (98.75DEG + 0.25HF + 1H_2O) increases from 0.386 to 0.403 N/m for 56 h, whereas with the same electrolytes, the TiO_2 nanotube array substrate shows perfect hydrophilic conditions. It is known that the chemical process and the operating conditions during the growth of the nanotubes have the ability to alter the surface tension and the contact angle in comparison to those measured values under *ex situ* sessile and

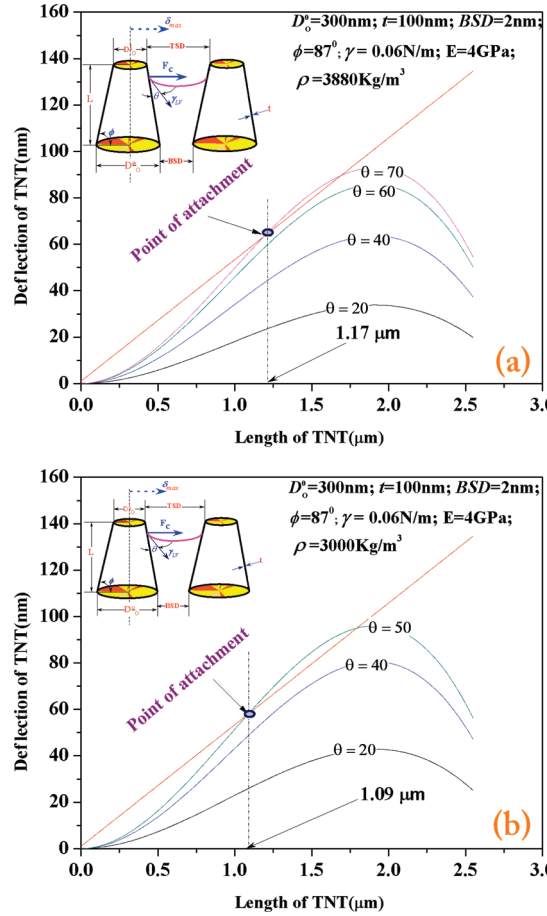

Figure 6. Variation in the deflection of the nanotube with the increment in the length of the nanotubes under different contact angle conditions assuming the density of amorphous anodized TiO_2 to be (a) 3.88 g cm^{-3} and (b) 3 g cm^{-3}. BSD and TSD are the base separation distance and tip separation distance, respectively.

pendant drop methods. Also, the nanoscopic surface roughness of the tube walls[41] affects imbibition, and their surface charge[42] can influence the contact angle of the liquid on the nanotubes. However, we ignore these effects in our simplified model. Hence, it is conceivable that the actual value of surface tension and contact angle are within the prescribed limits of those presented in Figure 6. Such a process-dependent change in contact angle for completely hydrophilic surfaces has been reported in the literature.[43,44]

There are reports of branched pores in anodically formed nanoporous alumina[45] and nanotubular titania.[46] In those reports, the branched pores with the inverted Y configuration were the result of modifying the growth parameters such as the anodization voltage or the temperature during anodization. In our case, we do not deliberately modify any growth parameters during the anodization. Furthermore, the operating mechanism is entirely different—we have shown that the nanotubes are grown in a nonbranched fashion and become branched due to a process called nanotube combination. In our process, distinct nanotubes combine together, which is why we call the structures mul-

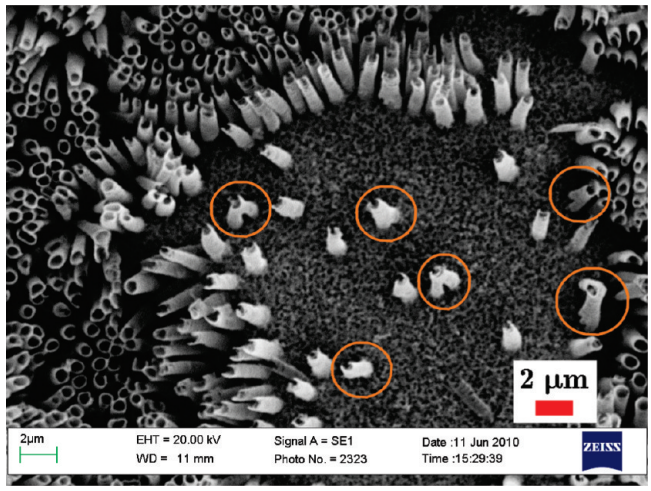

Figure 7. SEM image of the surface of a Ti foil anodized in a DEG-based electrolyte containing 0.25% HF and 1% H_2O for 45 h at 120 V. Similar to Figure 3, two distinct regions consisting of close-packed and widely separated nanotubes are seen; however, the chemical dissolution of the widely separated NT region is more advanced. Note how a majority of the surviving nanotubes in the chemically etched region are multipodal (orange circles point to obvious multipodal nanotubes; other surviving NTs are likely multipodal, too, but with one or more legs obscured).

tipodal nanotubes instead of branched nanotubes. An important consequence of the mechanism being different is the ability to form multipodal nanotubes wherein the angle between the constituent nanotubes (branches) is large (>20°). SEM images in Figure 1c,d and Figure 7 show several multipodal nanotubes where this angle is large. On the contrary, in the branching process reported in other papers (inverted Y), only a very narrow range of internanotubular angles are possible.

Nanotube combination efficiently allocates scarce fluoride-bearing species since two or more nanotubes can obtain fluoride-bearing species from the same puddle of bulk electrolyte after nanotube combination. Consequently, multipodal nanotubes that obtain access to fluoride-bearing species in the bulk electrolyte by the process of pore combination continue to grow subsequent to attachment (the Ti/TiO_2 interface below them keeps moving deeper into the Ti metal). This is clearly evident in Figure 7, where multipodal NTs are able to survive much longer than others subsequent to the first 40 h of anodization, when field-assisted processes weaken, leaving chemical etching dominant. This is why we propose that the weaker dissociation of HF, which results in fluoride ion scarcity, and the nature of the solvent (DEG in this case) used to form the electrolyte are the critical factors for nanotube combination. When ammonium fluoride (which has higher dissociation) and tetrabutyl ammonium fluoride (which dissociates completely) are used instead of HF as the fluoride-bearing species in the anodization electrolyte, F^- ions are not scarce, the formed nanotubes remain close-packed for very long anodization durations, and the diameters are capped at ~300 nm. We observe the formation of multipodal nanotubes in a narrow window of process parameters in DEG electrolytes: anodization voltages of 120 V or greater, anodization durations >40 h, and HF concentrations lower than 0.5%.

EXPERIMENTAL DETAILS

Anodic Growth. Titania nanotube arrays were obtained by anodization of a 0.25 mm thick titanium foil (99.7%, Sigma Aldrich) in a two-electrode anodization setup in which titanium foils were used as both the anode and cathode and only half of their length was immersed into the solution. Titanium foils were cleaned ultrasonically prior to anodization with soap, deionized water, and isopropyl alcohol and were dried with nitrogen gas. Anodization was carried out at room temperature in an electrolyte consisting of a mixture of DEG (Fisher Chemical), HF (48% solution, Sigma Aldrich), and deionized water under the applied voltages of 120 and 150 V. The electrochemical cell had a closed lid to reduce variation in electrolyte concentration with time, and the anodization was performed inside a fume hood with the sash half-closed. After anodization, the titanium foils containing the nanotubes were rinsed with isopropyl alcohol and dried in air. Subsequently, the cleaning process was completed by immersing the foils into 0.1 M HCl acid for an hour and drying it in the oven for 1 h at 100 °C.

Characterization. Morphology of the nanotubes including their length, diameter, wall thickness, and separation was investigated using a scanning electron microscope (SEM, ZEISS) as well as a field-emission scanning electron microscope (FESEM, JEOL 6301F). Contact angles with the sessile drop technique and the surface tension with pendant drop technique were measured using Krüss DSA 100 (Krüss GmbH, Hamburg, Germany). For the surface tension measurement, electrolytes of different degree of aging were selected, whereas the contact angle of a fresh electrolyte on various TiO_2 substrate was measured. In the case of surface tension measurement, an image of a drop in hydromechanical equilibrium condition is captured. DSA drop shape analysis, in-built software in the Krüss DSA 100 system, was used for the image processing to determine the surface tension and contact angle of the electrolytes. The software relies on the derivation of surface tension based on the Laplace pressure equation. As the hydromechanical equilibrium condition of the pendant drop is a more important parameter than the drop volume, the change in the drop volume was ignored during the surface tension measurement. Five measurements on each sample with a specific degree of aging were taken, and the average surface tension of the corresponding electrolytes was determined. For the contact angle measurement, the drop was disposed from needle to obtain a sessile drop on the substrate. It was observed that the substrate shows perfect wetting conditions. Further details of such measurement procedure can be found elsewhere.[47]

Acknowledgment. K.S. was supported by a Suncor PetroCanada Young Innovator Award, a CFI LOF award, and start-up funds from the University of Alberta. All of the authors thank NSERC for financial support. Authors also acknowledge the staff of the Scanning Electron Microscopy Laboratory in the Department of Earth and Atmospheric Sciences (University of Alberta). Authors acknowledge funding provided to P.R.W. in the form of a scholarship by Alberta Ingenuity, now part of Alberta Innovates-Technology Futures, Province of Alberta.

Supporting Information Available: SEM images of the effect of pure chemical etching on TiO_2 in the absence of an applied anodization voltage. This material is available free of charge *via* the Internet at http://pubs.acs.org.

REFERENCES AND NOTES

1. Mor, G. K.; Shankar, K.; Paulose, M.; Varghese, O. K.; Grimes, C. A. Use of Highly-Ordered TiO_2 Nanotube Arrays in Dye-Sensitized Solar Cells. *Nano Lett.* **2006**, *6*, 215–218.
2. Zhu, K.; Neale, N. R.; Miedaner, A.; Frank, A. J. Enhanced Charge-Collection Efficiencies and Light Scattering in Dye-Sensitized Solar Cells Using Oriented TiO_2 Nanotube Arrays. *Nano Lett.* **2007**, *7*, 69–74.
3. Paulose, M.; Varghese, O. K.; Mor, G. K.; Grimes, C. A.; Ong, K. G. Unprecedented Ultra-high Hydrogen Gas Sensitivity in Undoped Titania Nanotubes. *Nanotechnology* **2006**, *17*, 398–402.
4. Varghese, O. K.; Yang, X. P.; Kendig, J.; Paulose, M.; Zeng, K. F.; Palmer, C.; Ong, K. G.; Grimes, C. A. A Transcutaneous Hydrogen Sensor: From Design to Application. *Sens. Lett.* **2006**, *4*, 120–128.
5. Shankar, K.; Basham, J. I.; Allam, N. K.; Varghese, O. K.; Mor, G. K.; Feng, X. J.; Paulose, M.; Seabold, J. A.; Choi, K. S.; Grimes, C. A. Recent Advances in the Use of TiO_2 Nanotube and Nanowire Arrays for Oxidative Photoelectrochemistry. *J. Phys. Chem. C* **2009**, *113*, 6327–6359.
6. Varghese, O. K.; Paulose, M.; LaTempa, T. J.; Grimes, C. A. High-Rate Solar Photocatalytic Conversion of CO_2 and Water Vapor to Hydrocarbon Fuels. *Nano Lett.* **2009**, *9*, 731–737.
7. Mor, G. K.; Kim, S.; Paulose, M.; Varghese, O. K.; Shankar, K.; Basham, J.; Grimes, C. A. Visible to Near-Infrared Light Harvesting in TiO_2 Nanotube Array-P3HT Based Heterojunction Solar Cells. *Nano Lett.* **2009**, *9*, 4250–4257.
8. Shankar, K.; Mor, G. K.; Paulose, M.; Varghese, O. K.; Grimes, C. A. Effect of Device Geometry on the Performance of TiO_2 Nanotube Array-Organic Semiconductor Double Heterojunction Solar Cells. *J. Non-Cryst. Solids* **2008**, *354*, 2767–2771.
9. Shankar, K.; Bandara, J.; Paulose, M.; Wietasch, H.; Varghese, O. K.; Mor, G. K.; LaTempa, T. J.; Thelakkat, M.; Grimes, C. A. Highly Efficient Solar Cells Using TiO_2 Nanotube Arrays Sensitized with a Donor-Antenna Dye. *Nano Lett.* **2008**, *8*, 1654–1659.
10. Popat, K. C.; Eltgroth, M.; La Tempa, T. J.; Grimes, C. A.; Desai, T. A. Titania Nanotubes: A Novel Platform for Drug-Eluting Coatings for Medical Implants. *Small* **2007**, *3*, 1878–1881.
11. Liu, H.; Wang, D.; Ji, L.; Li, J.; Liu, S.; Liu, X.; Jiang, S. A Novel TiO_2 Nanotube Array/Ti Wire Incorporated Solid-Phase Microextraction Fiber with High Strength, Efficiency and Selectivity. *J. Chromatogr. A* **2010**, *1217*, 1898–1903.
12. Park, J.; Bauer, S.; Schmuki, P.; von der Mark, K. Narrow Window in Nanoscale Dependent Activation of Endothelial Cell Growth and Differentiation on TiO_2 Nanotube Surfaces. *Nano Lett.* **2009**, *9*, 3157–3164.
13. von der Mark, K.; Bauer, S.; Park, J.; Schmuki, P. Another Look at "Stem Cell Fate Dictated Solely by Altered Nanotube Dimension". *Proc. Natl. Acad. Sci. U.S.A.* **2009**, *106*, E60.
14. *Nanoparticle Assemblies and Superstructures*; CRC Press: Boca Raton, FL, 2005.
15. Song, Y. Y.; Schmidt-Stein, F.; Bauer, S.; Schmuki, P. Amphiphilic TiO_2 Nanotube Arrays: An Actively Controllable Drug Delivery System. *J. Am. Chem. Soc.* **2009**, *131*, 4230–4232.
16. Svrcek, V.; Turkevych, I.; Hara, K.; Kondo, M. Ordered Titanium Dioxide Nanotubes Filled with Photoluminescent Surfactant-Free Silicon Nanocrystals. *Nanotechnology* **2010**, *21*, 215203.
17. Wang, Q.; Zhu, K.; Neale, N. R.; Frank, A. J. Constructing Ordered Sensitized Heterojunctions: Bottom-Up Electrochemical Synthesis of p-Type Semiconductors in Oriented n-TiO_2 Nanotube Arrays. *Nano Lett.* **2009**, *9*, 806–813.
18. Roy, S. C.; Paulose, M.; Grimes, C. A. The Effect of TiO_2 Nanotubes in the Enhancement of Blood Clotting for the Control of Hemorrhage. *Biomaterials* **2007**, *28*, 4667–4672.
19. Mohapatra, S. K.; Banerjee, S.; Misra, M. Synthesis of Fe_2O_3/TiO_2 Nanorod−Nanotube Arrays by Filling TiO_2 Nanotubes with Fe. *Nanotechnology* **2008**, *19*, 7.
20. Meng, G. W.; Jung, Y. J.; Cao, A. Y.; Vajtai, R.; Ajayan, P. M. Controlled Fabrication of Hierarchically Branched Nanopores, Nanotubes, and Nanowires. *Proc. Natl. Acad. Sci. U.S.A.* **2005**, *102*, 7074–7078.
21. Sugunan, A.; Jafri, S. H. M.; Qin, J.; Blom, T.; Toprak, M. S.; Leifer, K.; Muhammed, M. Low-Temperature Synthesis of Photoconducting CdTe Nanotetrapods. *J. Mater. Chem.* **2009**, *20*, 1208–1214.
22. Zhang, Q.; Fan, W.; Gao, L. Anatase TiO_2 Nanoparticles Immobilized on ZnO Tetrapods as a Highly Efficient and Easily Recyclable Photocatalyst. *Appl. Catal. B* **2007**, *76*, 168–173.
23. Hsu, Y. F.; Yip, C. T.; Djurisic, A. B.; Chan, W. K. Efficiency Enhancement for ZnO Tetrapod Dye-Sensitized Solar Cells by TiO2 Coating and Ammonium Treatment. *2nd IEEE International Nanoelectronics Conference*, 2008; pp 358−361.
24. Mohammadpour, A.; Shankar, K. Anodic TiO_2 Nanotube Arrays with Optical Wavelength-Sized Apertures. *J. Mater. Chem.* **2010**, *20*, 8474–8477.
25. Yoriya, S.; Grimes, C. A. Self-Assembled TiO_2 Nanotube Arrays by Anodization of Titanium in Diethylene Glycol: Approach to Extended Pore Widening. *Langmuir* **2010**, *26*, 417–420.
26. Yoriya, S.; Mor, G. K.; Sharma, S.; Grimes, C. A. Synthesis of Ordered Arrays of Discrete, Partially Crystalline Titania Nanotubes by Ti Anodization Using Diethylene Glycol Electrolytes. *J. Mater. Chem.* **2008**, *18*, 3332–3336.
27. Mor, G. K.; Varghese, O. K.; Paulose, M.; Mukherjee, N.; Grimes, C. A. Fabrication of Tapered, Conical-Shaped Titania Nanotubes. *J. Mater. Res.* **2003**, *18*, 2588–2593.
28. Yasuda, K.; Macak, J. M.; Berger, S.; Ghicov, A.; Schmuki, P. Mechanistic Aspects of the Self-Organization Process for Oxide Nanotube Formation on Valve Metals. *J. Electrochem. Soc.* **2007**, *154*, C472–C478.
29. Sivaprasad, P.; Kalidas, C. Conductance Behavior of HCl in Water-Ethylene Glycol, Water-Diethylene Glycol and Ethylene Glycol-Diethylene Glycol Mixtures. *Proc. Indiana Acad. Sci.* **1983**, *92*, 203–209.
30. Shankar, K.; Mor, G. K.; Fitzgerald, A.; Grimes, C. A. Cation Effect on the Electrochemical Formation of Very High Aspect Ratio TiO_2 Nanotube Arrays in Formamide−Water Mixtures. *J. Phys. Chem. C* **2007**, *111*, 21–26.
31. Izutsu, K. *Electrochemistry in Nonaqueous Solutions*; Wiley-VCH Verlag GmbH & Co.: Weinheim, Germany, 2003.
32. Macak, J. M.; Schmuki, P. Anodic Growth of Self-Organized Anodic TiO_2 Nanotubes in Viscous Electrolytes. *Electrochim. Acta* **2006**, *52*, 1258–1264.
33. Sun, L. D.; Zhang, S.; Sun, X. W.; He, X. D. Effect of Electric Field Strength on the Length of Anodized Titania Nanotube Arrays. *J. Electroanal. Chem.* **2009**, *637*, 6–12.
34. Sreekantan, S.; Saharudin, K. A.; Lockman, Z.; Tzu, T. W. Fast-Rate Formation of TiO_2 Nanotube Arrays in an Organic Bath and Their Applications in Photocatalysis. *Nanotechnology* **2010**, *21*, 365603.
35. Prakasam, H. E.; Shankar, K.; Paulose, M.; Varghese, O. K.; Grimes, C. A. A New Benchmark for TiO_2 Nanotube Array Growth by Anodization. *J. Phys. Chem. C* **2007**, *111*, 7235–7241.
36. Kalidas, C.; Rao, V. S. Conductance of Hydrogen Halides in Diethylene Glycol at Different Temepratures. *Indian J. Chem. A* **1976**, *14*, 129–131.
37. Rao, V. S.; Kalidas, C. Effect of Water on Conductance of Hydrogen Halides in Diethylene Glycol. *Bull. Chem. Soc. Jpn.* **1976**, *49*, 203–205.
38. Zhu, K.; Vinzant, T. B.; Neale, N. R.; Frank, A. J. Removing Structural Disorder from Oriented TiO_2 Nanotube Arrays: Reducing the Dimensionality of Transport and Recombination in Dye-Sensitized Solar Cells. *Nano Lett.* **2007**, *7*, 3739–3746.
39. Roy, P.; Dey, T.; Schmuki, P. Scanning Electron Microscopy Observation of Nanoscopic Wetting of TiO_2 Nanotubes

and ODS Modified Nanotubes Using Ionic Liquids. *Electrochem. Solid State* **2010**, *13*, E11–E13.
40. Van Hoang, V. The Glass Transition and Thermodynamics of Liquid and Amorphous TiO_2 Nanoparticles. *Nanotechnology* **2008**, *19*, 105706.
41. Stukan, M. R.; Ligneul, P.; Crawshaw, J. P.; Boek, E. S. Spontaneous Imbibition in Nanopores of Different Roughness and Wettability. *Langmuir* **2010**, *26*, 13342–13352.
42. Hill, J. J.; Haller, K.; Gelfand, B.; Ziegler, K. J. Eliminating Capillary Coalescence of Nanowire Arrays with Applied Electric Fields. *ACS Appl. Mater. Interfaces* **2010**, *2*, 1992–1998.
43. Pinzari, F.; Ascarelli, P.; Cappelli, E.; Mattei, G.; Giorgi, R. Wettability of HF-CVD Diamond Films. *Diam. Relat. Mater.* **2001**, *10*, 781–785.
44. Kim, D.; Macak, J. M.; Schimidt-Stein, F.; Schmuki, P. Capillary Effects, Wetting Behavior and Photo-induced Tube Filling of TiO_2 Nanotube Layers. *Nanotechnology* **2008**, *19*, 305710.
45. Li, J.; Papadopoulos, C.; Xu, J. Nanoelectronics—Growing Y-Junction Carbon Nanotubes. *Nature* **1999**, *402*, 253–254.
46. Mohapatra, S. K.; Misra, M.; Mahajan, V. K.; Raja, K. S. Synthesis of Y-Branched TiO_2 Nanotubes. *Mater. Lett.* **2008**, *62*, 1772–1774.
47. Waghmare, P.; Mitra, S. K. Contact Angle Hysteresis of Microbead Suspensions. *Langmuir* **2010**, *26*, 17082–17089.